Nanoscale

Accepted Manuscript

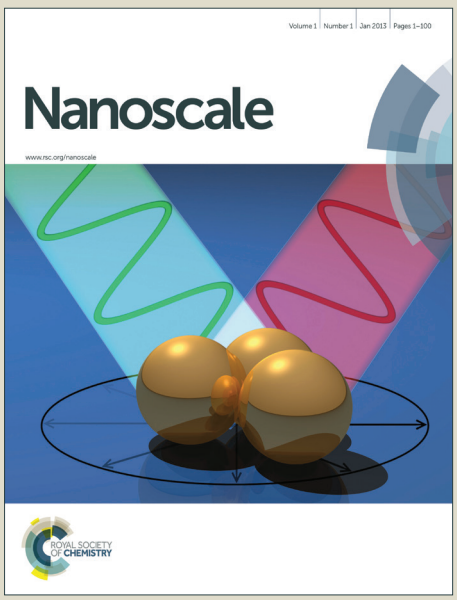

ROYAL SOCIETY OF CHEMISTRY

www.rsc.org/nanoscale

Nanoscale

RSCPublishing

ARTICLE

Integration of Nanostructured Dielectrophoretic Device and Surface-Enhanced Raman Probe for Highly Sensitive Rapid Bacteria Detection

Foram Ranjeet Madiyar[a], Saheel Bhana[b], Luxi Swisher[a], Xiaohua Huang[b], Christopher Culbertson[a], and Jun Li[a]

Abstract: This work reports a synergistic approach for the concentration, detection and kinetic monitoring of pathogens through the integration of nanostructured dielectrophoresis (DEP) with nanotag-labelled Surface Enhanced Raman Scattering (SERS). A nanoelectrode array made of embedded Vertically Aligned Carbon Nanofibers (VACNFs) at the bottom of a microfluidic chip was used to effectively capture and concentrate nanotag-labelled *E. coli* DHα5 cells into a 200 μm x 200 μm area on which a Raman laser probe was focused. The SERS nanotags were based on iron oxide-gold (IO-Au) core-shell nanoovals (NOVs) of ~50 nm in size, which were coated with a QSY21 Raman reporter and attached to *E. coli* through specific immunochemistry. The combination of the greatly enhanced Raman signal by the SERS nanotags and the effective DEP concentration significantly improved the detection limit and speed. The SERS signal was measured with both a confocal Raman microscope and a portable Raman probe during DEP capture, and was fully validated with fluorescence microscopy measurements under all DEP conditions. The SERS measurements were sensitive enough to detect a single bacterium. A concentration detection limit as low as 210 cfu/mL using a portable Raman system was obtained with a DEP capture time of only ~50 s. These results demonstrate the potential to develop a compact portable system for rapid and highly sensitive detection of specific pathogens. This system is reusable, requires minimum sample preparation, and is amenable for field applications.

1.0 Introduction

Infection by pathogenic microorganisms, such as bacteria, viruses and protozoa, is a widespread and significant public health problem. Besides implementing strict hygienic regulations, the development of new techniques for rapid and highly sensitive pathogen detection is critical to limit the spread of the pathogens and to reduce the potential damage. Conventional culture methods, although sensitive, are often too slow, take hours to days to obtain the results, and lack specificity.[1, 2] Molecular methods including immunoassays[3] and nucleic acid analysis[4] may be sensitive and specific but require bulky laboratory instruments and lengthy sample preparation procedures. Therefore, none of these current methods are applicable for rapid surveillance and in-field screening.[1, 2] Nanotechnology has been extensively explored for its potential in developing miniaturized nanobiosensors with enhanced detection speed and sensitivity. This has resulted in the use of suspended micro and nanoparticles in a range of in-situ Raman measurement techniques.[5-10] In this work, we integrate two nanotechnologies into a portable system, i.e. (1) a nanoelectrode array (NEA) embedded in a fluidic chip for highly localized dielectrophoretic (DEP) capture/concentration of bacteria, and (2) a surface enhanced Raman spectroscopy (SERS) probe for specific bacteria identification. We demonstrate that this method can be potentially developed into a highly sensitive portable system for rapid in-field pathogen detection.

SERS employs greatly enhanced electromagnetic fields in the vicinity (<10 nm) of a nanostructured metal substrate surface to interact with molecules adsorbed on the substrate surface.[11, 12] The Raman scattering intensity may be enhanced up to 14 to 15 orders of magnitude at certain hot spots.[13, 14] Various SERS methods have

been developed for powerful non-destructive spectroscopic investigation of molecular structures.[11, 12] In addition, SERS can identify specific vibrational frequencies of the chemical functionalities in complex aqueous biological samples with convenient visible and near infrared laser probes. There is a strong interest in developing portable SERS systems for pathogen detection.[15, 16]

There are two general approaches for SERS based pathogen detection.[15] The first is direct detection of the intrinsic vibrational fingerprint of a pathogen by bringing the pathogen in close proximity to a metallic nanostructure (e.g. colloidal nanoparticles,[17] nano-clusters,[18] sandwich structures of gold film and nanoparticles[19] and controlled nano-structured substrates[20]). Using this approach and a novel barcode Raman data processing procedure, ~10 bacteria can be detected in a solution.[21, 22] However, the direct identification of pathogens requires a highly controlled SERS substrate in combination with reproducible spectral data, as pathogen identification is accomplished by processing data using statistical algorithms that analyse minute differences in the Raman spectra. This turns out to be very challenging due to two factors: (1) the strong dependence of SERS signal on the surface structure, size/shape of the nano-structured substrate, the excitation laser wavelength, and the configurations of pathogen binding on the nanostructure surface;[23, 24] and (2) the fast exponential decay of the electromagnetic field away from the nanostructure surface.[25] All these variables lead to a lack of consistency and poor reproducibility of the SERS measurements.

The second approach is an indirect detection method using a SERS nanotag as a quantitative reporter.[16] The SERS nanotag is a complex structure consisting of a nanoscale metallic substrate attached to a molecule with a strong, unique Raman fingerprint. The pre-fabricated nanotag complex ensures that the reporter molecules are in close contact with metal nano-substrates to give a high surface enhancement. In addition, the nanotags are co-functionalized with biorecognition molecules (such as antibodies, aptamers, etc.) which specifically bind to the pathogens. As a result, the high SERS signal is only obtained from a specific pathogen and not from other microorganisms. The specific identification of a pathogen can thus be achieved without relying on multivariate analysis. Several previous reports have demonstrated the use of 4-mercaptobezoic acid[26], [5,5′-dithiobis(succinimidyl-2-nitrobenzoate)] (DSNB)[16, 27], tetramethylrohodamine isothiocynate (TRITC) and QSY21 dye[28] as effective Raman markers.

In this study, we focus on the specific detection of *E. coli* strain Dhα5 using the SERS reporter QSY21 that is co-functionalized with polyclonal antibodies on anisotropic oval-shaped iron oxide-gold (IO-Au) core-shell nanoparticles. The irregular shape and thickness of the Au shell provides a large enhancement factor for SERS.[22, 23] In order to further lower the detection limit and simplify the sample preparation, the *E. coli* are concentrated by DEP into a 200 μm x 200 μm area inside a fluidic channel where the Raman laser beam is aligned and focused. An NEA made of vertically aligned carbon nanofibers (VACNFs)[29] at the bottom of this area versus a macroscopic indium tin oxide (ITO) transparent electrode at the top form the DEP device in a "point-and-lid" geometry[30]. As we demonstrated before, a moderate AC voltage applied between the NEA and the ITO electrode can effectively capture bacteria[31, 32] or viral particles[33, 34] due to the greatly enhanced electric field at the exposed VACNF tips. In the integrated system, we demonstrate the use of this fast, active and reversible concentration technique to bring bacteria into the field of view of a fixed Raman probe. Highly sensitive SERS detection is demonstrated with both a confocal Raman microscope and a portable Raman system as very dilute solutions of bacteria are passed through the fluidic chip.

2.0 Results and Discussion

2.1 Experimental Design DEP was first described by Pohl in 1966[35] and has been widely used in biology to separate live and dead bacteria,[35, 36, 37] viruses,[33] cells,[38] and DNA. Generally, DEP is based on a spatially non-uniform electric field generated by an AC voltage bias between a pair of electrodes, resulting in a time average net force on neutral polarizable particles that depends on the permittivity and conductivity of the particle and medium.[35] The DEP force (F_{DEP}) acting on the spherical particles by the non-uniform electric field is given by:

$$\langle F_{DEP} \rangle = 2\pi r^3 \varepsilon_m \mathrm{Re}[K(\omega)] \nabla E^2, \quad (1)$$

where r is the radius of the particle, ε_m is the permittivity of the suspending medium, ∇E^2 is the gradient of the square of the applied electric field strength, and Re[$K(\omega)$] is the real component of the complex Clausius-Mossotti (CM) factor given by:

$$K(\omega) = \frac{\varepsilon_p^* - \varepsilon_m^*}{\varepsilon_p^* + 2\varepsilon_m^*}, \quad \text{where } \varepsilon^* = \varepsilon - j\frac{\sigma}{\omega} \quad (2)$$

with ε^* representing the complex permittivity and the indices p and m referring to particle and medium, respectively. Here σ is the conductivity, ω is the angular frequency of the applied electric field, and $j = \sqrt{-1}$. Re[$K(\omega)$] describes the frequency dependence of the polarizabilities of a particle in the field which is positive if the particle is more polarizable than the surrounding medium. The force is then directed toward regions of high field strength, which is known as positive DEP (pDEP). A system with negative value of Re[$K(\omega)$] will push the particles toward lower electric field strength. The value of Re[$K(\omega)$] of a bacteria in an aqueous medium can vary from -0.5 to 1.0, depending on the effective polarizabilities of particle and medium. In this study large pDEP is desired to capture bacteria at the exposed VACNF tip by selecting a proper frequency and the right medium composition.

The direct detection of a bacterium fingerprint using SERS has been studied before using circular ring electrodes,[39] quadrupole electrodes[40] and curved electrodes[41]. In this study based on indirect detection, QSY21 Raman reporter was used because it strongly adsorbed to the negatively charged surface of gold-coated-IO nanoovals (NOVs) through electrostatic interactions.[42, 43] The dye has highly delocalized pi-electrons and the anisotropic shape of the NOVs gives strong SERS signals.[42] A schematic representation of the experimental set-up using a confocal Raman microscope is shown in Fig. 1. In this setup, a 780 nm laser was focused at the exposed VACNF tips in the active DEP area to probe the captured *E. coli* DHα5 cells and obtain SERS spectrum of QSY21 from the bound nanotags. More details are shown in Fig. S1 of supplementary information.

Fig. 2 summarizes the procedure to prepare the SERS nanotag nano-ovals (NOVs) that bind to *E. coli* DHα 5. In brief, the NOVs were synthesized from spherical IO nanoparticle cores (~23 nm diameter) onto which an irregular-shaped Au shell was deposited, forming NOVs with the outer dimension of 35 to 50 nm to provide a large

SERS enhancement factor.[42, 43] The NOV surfaces were then coated with a mixture of carboxy-polyethylene glycol-thiol (HOOC-PEG-SH, MW 5000) and methoxy-polyethylene glycol-thiol (mPEG-SH, MW 5000) in order to make NOVs biocompatible, stabilize the QSY21 adsorption, and to introduce carboxylic acid groups at the surface for covalent attachment of a Alexa 555-labelled secondary antibodies through amide bond formation. The *E. coli*-specific primary antibody (labelled with FITC for fluorescence validation) was then bound to the secondary antibody on IO-Au SERS NOVs to form the completed SERS nanotag. Before each experiment, these SERS nanotags were mixed with the bacteria sample to allow for the attachment of the nanotag to *E. coli* bacteria through specific immunochemistry. The structure of QSY21 and its typical Raman spectrum is shown at the center of Fig. 2. Raman bands at 1333, 1584 and 1641 cm^{-1} are from the xanthene ring stretching vibrations of the molecule.[44] The strongest characteristic band is seen at 1496 cm^{-1}. The signal from the QSY21 attached to the NOV nanotag for this band demonstrates an enhancement factor of 4.9 x 10^4 over a 0.1 mM solution of QSY21[28] and thus is used in this study for the quantitative measurement. Figs. 2b and 2c show TEM images of IO-Au SERS NOVs and those bound onto *E. coli*. On average, there are hundreds of NOVs bound to each *E. coli*, which gives a Raman signal sufficient to be detected at the single cell level. The confocal fluorescence microscopy image of Alexa 555 dye labelled secondary antibody on the *E. coli* cells (Fig. 2d) clearly illustrates the uniform coating of NOVs on *E. coli* DHα5 through specific immunochemical binding.

2.2 Raman Detection and DEP Optimization To validate and optimize the conditions, DEP capture was first monitored under a confocal Raman microscope at various flow velocities (Fig. 3a) and AC voltage frequencies (Fig. 3f). The results were compared side-by-side with the video of Alex 555 (in the functionalized secondary antibody) under a fluorescence microscope following our previously established method.[32, 33] The Raman intensity is the signal at the Raman shift of 1496 cm^{-1} corresponding to the peak of the QSY21 reporter. Figs. 3b and 3g are representative Raman spectra of QSY21 at different flow velocities and AC frequencies. The representative snapshots from a fluorescence video during DEP capture of the NOV-bound bacteria within the 200 μm × 200 μm active NEA area are shown in Figs. 3c to 3e (see supplementary information for the full videos).

Similar to our previous report on *E. coli* capture[27], the AC voltage V_{pp} was turned on for 50 s while the bacteria/IO-Au NOVs solution was passed through the channel. The bacteria were collected at randomly distributed VACNF tips which have the highest ∇E^2. Both the fluorescence and SERS signals associated with the captured bacteria were found to increase nearly linearly with time. The difference between the integrated fluorescence intensity (ΔF) at the end of the 50 s capture period with that right before application of the capture voltage was used to quantitatively determine the DEP capture efficiency. The pDEP capture experiments were carried out at flow velocities (v) ranging from 0.11 to 2.43 mm/s using a fixed AC voltage of 10 V_{pp} and frequency of 100 kHz. The number of captured bacteria initially increased with increasing flow rate until a maximum was reached at 0.33 mm/s (corresponding to volumetric flow rate of 0.5 μL/s). Further increases in flow velocity resulted in a decrease in capture efficiency. The trend agrees well with our previous study.[27] An image of the final video frame taken for the capture efficiency experiment using the 0.33 mm/s flow rate is shown in Fig. 3d. The bright spots generally represent single captured bacterium. Raman intensity follows the same trend as the fluorescence measurements. At $v \geq 0.33$ mm/s (Fig. 3a), the number of captured *E. coli* DHα5 cells decreased because fewer cells can sustain the higher drag force of the fluidic flow. Only a small number of cells retain captured.

Because of the dependence of F_{DEP} (Eq 1 and 2) on the permittivity of a particle, each type of bio-particle has an optimum DEP frequency depending on its internal composition and structure. As shown in Fig. 3f, both fluorescence and SERS intensity show optimum DEP capture of the NOV-labelled *E. coli* DHα5 cells at ~100 kHz with fixed peak-to-peak voltage of 10 V_{pp} and a flow velocity of 0.33 mm/s. The optimum frequency was the same as that for bare *E. coli* DHα5 cells[32], indicating that the attachment of IO-Au NOVs on the bacteria surface did not alter their overall DEP properties. In contrast, Fig. S2 shows that the NOVs alone were not captured via DEP forces at ~100 kHz. Rather they were captured weakly at an optimum frequency of 10 kHz. The possibility that the measured SERS signal was from free NOV nanotags, therefore, was excluded. Combining these observations, it is clear that SERS detection with NOV nanotags is viable and highly sensitive for monitoring the DEP capture of labelled *E. coli* DHα5 cells.

The magnitude of ∇E^2 depends on both of the DEP device design and the amplitude of the applied AC voltage. Low voltage capture is preferred for bioparticles to prevent potential cellular damage. Fig. 4a shows results with the voltage varying between 3 to 10 V_{pp} while other parameters were fixed at the optimized conditions, i.e. flow velocity of 0.33 mm/sec and frequency of 100 kHz. The DEP capture indicated by SERS and fluorescence signals increased monotonically with the voltage and showed strong capture at 10 V_{pp}. But a large SERS signal was observed even at 6 V_{pp} (Figs. 4b and 4c).

Fig. 4c shows the kinetic curves of DEP capture at a low *E. coli* concentration of 5.4 x10^3 cfu/ml. Both of the fluorescence and SERS signals slowly increase after the voltage was turned on since the number of available bacteria was limited by the mass transport. The bacteria were immediately released when the AC voltage was turned off. Thus the device can be repeatedly used. The kinetic curve based on the SERS signal was further converted into the number of captured *E. coli* cells by dividing the measured SERS intensity by the average SERS intensity from a single NOV-labelled *E. coli* cell that was measured in a separate quartz cell-counting chamber. The Raman intensity of individual bacterium was measured using a *Petroff-Hausser* counting chamber made of quartz. The bacteria sample was diluted so that the individual bacterium was far apart and fixed in position. The excitation laser was focused on the cells one by one for confocal Raman measurements. The obtained average Raman intensity of an individual bacterium was 32.5 ± 4.6 a.u., showing a small variation due to the random fluctuation in the number of attached IO-Au NOV nanotags. The Raman kinetic curve showed a nearly a step-wise increase as single *E. coli* cells were captured. As illustrated in Fig. 4d, the small size of the laser spot (3.1 μm in diameter) likely limited the maximum number of measurable bacteria to only ~4 within this spot. Clearly, a single *E. coli* cell can be easily detected with this device as long as they can be brought under the laser probe.

2.3 Assessment of DEP capture in complex matrix samples In order to demonstrate the capability of the DEP capture and SERS detection of bacterial cells in complex samples, *E. coli* cells were spiked into chicken broth, apple juice and soil solution for testing. Complex matrices present different challenges due to the presence of inorganic and organic substance which may interact with the bacterial cells, antibodies, or SERS nanotags, making it different from the pure bacteria solutions. Additional preparation procedures

including washing, centrifugation and filtration (with 0.22 μm membrane) of the complex samples were applied before they were spiked with 5 x 10^5 cfu/ml *E. coli* cells. These commonly used sample preparation procedures are necessary to eliminate larger particles that can clog the micro-channels. The conductivity of bacteria in distilled water (pH 6.8) was 1.22 x 10^{-4} S/m. The conductivity of the commercial chicken broth (pH 7.22) was 0.45 S/m. The presence of salt in the chicken broth caused the high conductivity but was largely removed during sample preparation. After the sample processing procedures, *E. coli* DHα5 cells were added and resulted in a conductivity of 1.7 x 10^{-3} S/m (pH = 7.13). The soil solution (pH = 4.58) had a conductivity of 0.027 S/m in the raw sample, which dropped to 2.35 x 10^{-4} S/m (pH = 6.8) after the preparation and *E. coli* spiking. For the apple juice, the conductivity was 0.155 S/m in the raw sample (pH = 2.95) and became 0.158 S/m (pH = 2.81) after the sample preparation and addition of *E. coli* cells.

Fig. 5 shows the real-time Raman measurements during DEP capture of 5 x 10^5 cfu/ml *E. coli* DHα5 cells spiked in the complex matrices at the frequency of 150 kHz and the flow velocity of 0.44 mm/s. To judge non-specific binding of the NOVs to the complex matrices, the conjugate NOV nanotags were added to chicken broth in a control experiment. Another control study was done with the processed complex matrices alone. Clearly, *E. coli* DHα5 cells can be captured by DEP and detected with SERS using the NOV nanotags in both chicken broth and the soil solution. The interference and nonspecific signal of the matrices were negligible. Systematic optimization by varying the frequency and flow velocity in these two complex matrices are presented in Fig. S3 in Supplementary Information. The results were very similar to those in distilled water (Fig. 3), only with the optimum AC frequency at 150 kHz in chicken broth in contrast to 100 kHz in distilled water and the soil solution. These are distinct from that of the conjugated NOVs spiked in respective matrices at a concentration of 1.4 x 10^{10} NOVs/mL. However, p-DEP capture of the bacteria was not observed in apple juice. This may be due either to the denaturization of the antibodies in the strong acidic solution (pH = 2.81 in the processed apple juice) preventing specific attachment of NOVs to bacteria or to the high conductivity of the apple juice resulting in negative value in Re[$K(\omega)$].

2.4 Assessment of Detection Sensitivity in a Portable System To demonstrate the potential capability of this method for use as a portable system, similar studies including flow velocity and frequency optimization were carried out with a portable Raman instrument (ProRaman L, Enwave Optronics. Inc.) in a manner similar to the earlier studies using the confocal Raman microscope. The results between these two Raman systems were very consistent, with the maximum flow velocity at 0.4 mm/sec (0.55 μl/s) and the maximum frequency at 100 kHz (see Fig. S4a and b in Supplementary Information). However, the probe diameter at the focal point in the portable Raman system is about 100 μm (Fig. S4c and inset of Fig. 6), which is much larger than the 3.1 μm size in the confocal Raman microscope (Fig. 4d). This allows signals to be collected from many more bacteria and yields better statistics, but the laser intensity is lower as it is spread over a larger area. These two factors need to be balanced for the optimum performance. DEP capture kinetic curves over longer time (~250 s) at higher concentration (5 x10^6 cfu/ml) show a similar nearly linear increase in fluorescence and Raman signals over DEP time (see Fig. S4d).

Figure 6 summarizes the SERS intensity of the captured NOV-labelled *E. coli* using the portable Raman setup while the *E. coli* concentration was varied from ~10 to 1 x 10^9 cfu/ml. The intensity of the QSY21 marker at the Raman shift of 1496 cm^{-1} could be clearly separated from the carbon nanofiber signals at 1350cm^{-1} (D-band) and 1600cm^{-1} (G-band), respectively. The Raman intensity was found to be a linear function of the logarithm of bacteria concentration when the concentration C is above ~100 cfu/ml as follows:

$$(\mathrm{RI})_{\mathrm{portable}} = 108.8 \times \log C - 214.7 \qquad (3)$$

$$(\mathrm{FI}) = 1224 \times \log C - 2650 \qquad (4)$$

where RI was the increase in Raman intensity collected from a 100 μm diameter DEP area and FI the increase in the integrated fluorescence intensity over the 200 μm x 200 μm active DEP area, respectively, after 50 s of DEP capture. It is surprising that the RI signal is proportional to log$C$ rather than directly proportional to C. The exact mechanism responsible for generating this relationship is not clear at this stage, but there are two possibilities to consider: (1) the rapid decay of the electric field at positions further away from the VACNF tip may generate a highly non-uniform DEP force (proportional to ∇E^2) that does not act equally on all cells in the whole solution volume between the NEA and ITO electrodes; or (2) the first captured bacteria may significantly screen the electric field and quickly lower the total DEP force on other cells in the solution. Overall, the larger size of the laser focal spot (100 μm in diameter) allowed the collection of Raman signals from a larger number of captured bacteria. But further increasing the Raman probe size to 300 μm gave a lower sensitivity, mainly due to lower excitation laser intensity as the power was spread out over a larger area.

For bacteria concentrations below the critical value C_0 = ~100 cfu/mL, no measurable signal above the background, i.e. $(RI)_{blank}$ = ~36 a.u., was detected. No captured bacterial cells were detected during the applied DEP period, which was limited by the slow mass transport of bacteria to the active area. But the Raman intensity increased as more bacteria were passed into the device at higher concentrations. The detection limit logC_{dl} was determined using calibration curve as follows:

$$\log C_{dl} = \log C_0 + 3\sigma_{blank}/m\,, \qquad (5)$$

where σ_{blank} (~11.7) is the standard deviation of the Raman signal for bacteria concentration below C_0 and m = 108.8 is the slope of the calibration curve. Thus the concentration detection limit was determined to be ~210 cfu/mL. For fluorescence measurement the σ_{blank} (~9.1) is the standard deviation of the fluorescence signal for bacteria concentration below C_0 (C_0 = ~500 cfu/ml, no measurable signal above the background) and m = 1224 the slope of the calibration curve. Thus the concentration detection limit for fluorescence measurements was determined to be ~827 cfu/ml (Figure S5 in Supplementary Information).

The optimum flow velocity of 0.4 mm/s corresponded to a volumetric flow rate of 0.55 μL/sec. For a 50 s DEP period, ~6 bacteria passed through the fluidic channel at the concentration detection limit of 210 cfu/mL. Even if the capture efficiency was only 15%, at least one bacteria would be captured, and this event would be detectable by SERS with this portable system. In the current DEP design, the 200 μm width of the active NEA array is much smaller than the total channel width (i.e. the 2 mm dia. circular chamber, see Fig. 1c) for the ease of aligning the NEA area within the fluidic channel. There detector design is, therefore, far from optimized since many bacterial cells may pass around the active DEP area and not be captured. In the future, the channel size and the

active DEP area will be reduced close to the Raman probe size so that all bacteria will be forced to pass through the active DEP zone so that they can be captured for Raman measurement. In addition, the DEP capture time can be increased from 50 s to several minutes to ensure more bacterial cells are captured. With such optimization, the concentration detection limit is expected to be lowered by a factor of 10, to ~10 cfu/mL.

3.0 Experimental

3.1 Materials and Methods Indium Tin Oxide (ITO) coated glass was purchased from Delta Technologies (Loveland, CO), SU-8 2010 and SU-8 2002 photoresist was purchased from Microchem (Newton, MA), conductive silver epoxy from MG Chemicals (Ontario), and microfluidic fittings from Upchurch Scientific Inc. (Oak Harbor, WA). QSY21 was purchased from Life Technologies (Grand Island, NY, USA). Carboxypoly (ethylene)-thiol (HOOC-PEG-SH, MW 5000) and methoxy-PEG-thiol (mPEG-SH, MW 5000) were purchased from Laysan Bio Inc. (Arab, AL, USA). *E. coli* DHα5 were purchased from Life Technologies (18265-017, Grand Island NY, USA). FITC conjugated rabbit anti-*E. coli* Rabbit primary antibody was purchased from AbD Serotech, (Raleigh, NC, USA), and Alexa 555 conjugated goat anti-rabbit secondary antibody was purchased from Invitrogen (Carlsbad, CA, USA).

3.2 DEP Device Fabrication Fabrication procedures and the fluidic geometry were similar to previous reports by Syed et.al.[32,33] Briefly, the device consisted of two electrodes on separate plates; namely an ITO lid electrode and an embedded VACNF NEA on an Si wafer. The two electrodes were arranged opposite to one another, separated by the fluidic channel. The fluidic channel was made on 1 cm x 2 cm diced ITO glass by spin coating SU-8 2010 photoresist at 1560 rpm for 40 s giving ~18 μm thickness (height). After soft baking on a hot plate for 4 min at 95 ^{o}C, the photoresist was exposed to UV light (32.9 mW/cm^2) for 7.61 s through a Mylar mask to define the microchannel (500 μm in width) with a circular chamber (~2 mm in diameter) at the center. After post-baking on a hot plate for 4 min at 95 ^{o}C, the chip was developed in SU-8 developer, washed with Iso-Propyl Alcohol (IPA) and dried in a stream of dry N_2. Two holes were drilled into the glass side at the two ends of the microchannel to serve as an inlet and outlet using a 0.75 mm diameter diamond drill bit. The embedded VACNF NEAs were fabricated by the method previously described.[29] The area exposed on the NEA (200 μm x 200 μm) was defined by another UV-lithography process. SU-8 2002 photoresist was spin-coated onto the VACNF chip at 2800 rpm for 40 s to produce ~2.0 μm thickness. The VACNF chip was then soft-baked at 95 ^{o}C for 75 s on a hot plate, exposed to UV light (32.9. mW/cm^2) for 3.98 s through a Mylar mask and post baked for 90 s on a hot plate at 95^{o}C. The next two steps were similar as described before. The two layers were aligned under 4X objective lens of a stereo microscope, pressed with mechanical force, and placed in a preheated vacuum oven (Curtin Matheson Scientific, Inc.) at 175 ^{o}C and a pressure of 25 Torr for ~30 min for the substrates to bond with each other. Electrical connections were made onto the NEA and ITO-glass using conductive silver epoxy and thirty gauge wires. Two microbore tubes were bonded at the 0.75 mm holes for fluidic inlet and outlet. A 1 ml glass syringe mounted on a syringe pump was used to control the flow rate through the inlet tubing during the experiments.

3.3 Preparation of antibody-conjugated IO-Au NOV SERS nanotags QSY21 adsorbed IO-Au NOVs was stabilized with HOOC-PEG-SH and mPEG-SH following the previous reported methods.[42] For ligand conjugation with Alexa 555 conjugated goat anti-rabbit (secondary antibody), 100 μL IO-Au NOV SERS nanotags, 3 mg 1-Ethyl-3-(3-dimethylaminopropyl) carbodiimide (EDC) and 3 mg sulfo-N-hydroxysuccinimide (sulfo-NHS) were added to pH 5.5 MES buffer to make solution volume to 500 μL. The mixture was vortexed for 15 min, and spun down at 10,000 rpm for 10 min. The pellet was re-dispersed in 200 μL of 1 X Phosphate Buffered Saline (PBS, pH 7.4), followed by the addition of 20 μL of 0.2 mg/mL of the secondary antibody. The solution was vortexed for 2 h at room temperature to complete the coupling reaction, and then stored at 4˚C. Prior to use, the solution was centrifuged and washed with 1X PBS buffer 3 times to remove non-conjugated antibodies.

3.3 Conjugation of Bacteria with IO-Au NOV SERS nanotags Frozen *E. coli* DHα 5 stock was thawed and grown in LB medium in a sterile culture tube and incubated overnight at 37˚ C to reach a cell concentration of 2.5 x 10^9 cfu/mL. The cells were centrifuged at 5000 rpm for 5 min, the supernatant LB media was discarded, the pellet was re-suspended and washed in 1.0 mL 1X PBS thrice to eliminate the remaining ingredients of the LB media. A bacteria solution of 2.5 x 10^9 cfu/mL was incubated with 50 μl FITC conjugated rabbit anti- E. coli Ab (AbD Serotech, Raleigh NC, USA) at 330 μg/mL for 1 h at 4˚ C. The cells were then centrifuged, washed with deionized (DI) water and diluted to a final concentration of 9.5 x 10^4 cfu/mL. The bacteria and antibody-conjugated IO-Au NOV SERS nanotag solutions were mixed together at a ratio of 1.05 x 10^5 the NOVs to one bacteria. The solution was vortexed for 3 min and incubated overnight at 4˚C. To ensure that only bacteria-conjugated NOVs are spun down, the spin speed was kept low around 2000 rpm for 10 min and this process was repeated three times and finally suspended in water. Transmission Electron Microscope (TEM) images of the NOVs and bacteria functionalized with the NOVs were taken by adding 5 μL of suspension to a 400-mesh copper grid and dried at room temperature overnight. The grids were examined by TEM (FEI CM 100 with AMT digital capturing system).

3.4 Sample preparation in complex-matrix samples Chicken broth, soil solution, and apple juice were used to test the viability of detecting bacteria in complex samples. Kroger chicken chunks in broth (141g, Cincinnati, OH) was purchased from the local grocery store and the ingredient label indicated the presence of chicken chunks, water, less than 2 % of salt, modified corn starch and sodium phosphate. The soil sample was obtained from the lawn near Chemistry Department on Kansas State University campus and was soaked 50 ml of DI water overnight. About 2 g chicken chunks and 5 g solid soil were washed by DI water and vortexed for 2 min for four times and finally resuspended in 50 ml DI water. Mott's 100 % apple juice (8 oz. Plano, TX) was obtained from the local grocery store and the ingredients include water, concentrated apple juice and ascorbic acid. About 5 ml of apple juice was diluted to 10 ml with DI water to make the stock solution. Before spiking the solutions with *E.coli* cells, the solutions were centrifuged at 14,000 rpm for 10 min and the supernatant was passed through 0.22 μm sterile syringe filters (EMD Millipore, Billerica, MA). After processing, the solutions were cloudy indicating that the samples still contained complex matrices. *E.coli* DHα5 was added into these solutions to a concentration of 5 x 10^5 cfu/ml. The conductivity of the solutions before and after addition of the bacteria were recorded.

4.0 Experimental Set-up

4.1 Fluorescence- and Raman- DEP Experiments Fluorescence-DEP experiments were carried out on an upright fluorescence optical

microscope (Axioskop 2 FS plus; Carl Zeiss) in reflection mode with 50 X objective focused at 200 µm x 200 µm active area. Labelled bacteria *E. coli* DHα5 conjugated to the NOVs suspended in D.I water was injected into the channel to carry out DEP experiments. A filter set for Alexa 555 with an excitation wavelength of 540-552 nm and emission wavelength of 567-647 nm (filter set 20HE, Carl Zeiss) was used in connection with an Axio Cam MRm digital camera to record fluorescence videos at an exposure time of 0.7 s using a multi-dimensional acquisition mode in the Axio-vision 4.7.1 release software (Carl Zeiss MicroImaging, Inc). Two types of Raman systems were used. The first one was an upright Thermo Scientific DXR™ confocal Raman microscope equipped with a 10 X objective (NA is 0.25 and spot size of 3.1 µm) and 780 nm laser, with Omnic 8 software for data acquisition and analysis. A full spectral range of 3500-50 cm^{-1} with an accuracy of 2 cm^{-1} was captured with a cooled CCD. Parameters were set at 5 mW laser power, 50 µm slit width, 1 s exposure time for all experiments. The laser beam was focused at the exposed VACNF tips using carbon signals at 1350cm^{-1} (D-band) and 1600cm^{-1} (G-band) as the reference. The measurements were repeated at 25 different spots within the 200 µm x 200 µm active area for obtaining better statistics. The average value was reported. The second system was a portable Raman system (Pro Raman L, Enwave Optronics. Inc.) with a CCD detector cooled to -60ºC with spectral range from 3,300 cm^{-1} to 100 cm^{-1}. Parameters including 325 mW laser power, 1 s exposure time and 100 µm probe diameter at focus (NA 0.25) were fixed for all experiments. A function generator (Model 33120A, Hewlett Packard, Palo Alto, CA, USA) was used to generate different frequencies (*f*) of the sinusoidal AC voltage. A syringe pump (NE-1000) from New Era Pump Systems (Farmingdale, NY, USA) was used to produce various flow velocities. Each DEP experiment was performed in a span of 85 s during which no voltage (V_{off}) was applied in the initial ~10 s, followed with a fixed AC voltage at specific frequency in the next ~50 s (V_{on}), and then no voltage bias again (V_{off}) in the last ~25 s. Videos were recorded during each experiment. To perform the control experiments, the NOVs were conjugated with the secondary antibody (labelled with Alexa 555) and bacteria are conjugated with the primary antibody (labelled with FITC) were independently passed through the microfluidic channel. The results were monitored using the fluorescence microscope to determine the optimum frequency of the AC voltage. Fluorescence videos and Raman spectra were taken throughout the course of the experiment. Ten different spots from the active area were taken at each variable i.e. frequency, voltage, flow velocity, and concentration to ensure a good statistical sampling. Background and fluorescent light was subtracted using Omnic 8 software. In addition, the true linear flow velocities within the focal depth of the microscope from NEA surface in the 200 µm x 200 µm active area were calculated from the recorded videos

5.0 Conclusion

In conclusion, the integration of a DEP chip for bacteria concentration and SERS detection for specific microorganism identification has been demonstrated. The DEP based on a VACNF NEA acts as an effective and reversible electronic manipulation technique to rapidly concentrate bacteria into a micro-area from the solution flowing through the microfluidic channel. A highly sensitive SERS nanotag based on QSY21 adsorbed on IO-Au NOVs provides greatly enhanced Raman signals and specific recognition to *E. coli* DHα5 cell through highly selective immunochemical binding using two specific antibodies. The SERS signal measured with both of a confocal Raman microscope and a portable Raman system during DEP capture was fully validated with fluorescence measurements under all DEP conditions. This detection method yields a concentration detection limit of 210 cfu/mL using the portable Raman system, and 827 cfu/mL by fluorescence microscope which can be further improved. The results demonstrated the potential to develop a compact portable system for rapid and highly sensitive detection of specific pathogens in fields.

Acknowledgements

We thank the financial support by the US Department of Homeland Security Scientific Leadership Award grant # 2012-ST-062-000055 and Kansas Bioscience Authority through the Centre of Excellence for Emerging Zoonotic Animal Disease (CEEZAD) at Kansas State University. The authors thank Steven Klankowski, Levi Desilla and Kinjal Madiyar for helpful discussions and programming instrument for continuous scans.

The authors have declared no conflict of interest

Notes and References

a Department of Chemistry, Kansas State University, Manhattan, KS 66506

b Department of Chemistry, The University of Memphis, Memphis, TN 38152

Correspondence: Dr. Jun Li, Department of Chemistry, Kansas State University, USA. Email: junli@ksu.edu Fax: 785-532-6666

Electronic Supplementary Information (ESI) available

1. B. Swaminathan and P. Feng, *Annu. Rev. Microbiol.*, 1994, **48**, 401-426.
2. O. Lazcka, F. J. Del Campo and F. X. Munoz, *Biosens. Bioelectron.*, 2007, **22**, 1205-1217.
3. P. D. Skottrup, M. Nicolaisen and A. F. Justesen, *Biosens. Bioelectron.*, 2008, **24**, 339-348.
4. D. Call, *Critical Reviews in Microbiology*, 2005, **31**, 91-99.
5. D. Hou, S. Maheshwari and H.-C. Chang, *Biomicrofluidics*, 2007, **1**, 014106.
6. L. Chen and J. Choo, *Electrophoresis*, 2008, **29**, 1815-1828.
7. N. A. Abu-Hatab, J. F. John, J. M. Oran and M. J. Sepaniak, *Applied Spectroscopy*, 2007, **61**, 1116-1122.
8. A. E. Grow, L. L. Wood, J. L. Claycomb and P. A. Thompson, *Journal of Microbiological Methods*, 2003, **53**, 221-233.
9. R. Wilson, S. A. Bowden, J. Parnell and J. M. Cooper, *Analytical Chemistry*, 2010, **82**, 2119-2123.
10. Y. S. Huh, A. J. Lowe, A. D. Strickland, C. A. Batt and D. Erickson, *Journal of the American Chemical Society*, 2009, **131**, 2208-2213.
11. P. L. Stiles, J. A. Dieringer, N. C. Shah and R. R. Van Duyne, in *Annu.Rev.Anal.Chem.*, 2008, vol. 1, pp. 601-626.
12. K. A. Willets and R. P. Van Duyne, *Annu. Rev. Phys. Chem.*, 2007, **58**, 267-297.
13. H. K. J. Kneipp, A. Rajadurai, R.W. Redmond and K. Kneipp, *Journal of Raman Spectroscopy*, 2009, **40**, 1-5.
14. S. Nie and S. R. Emory, *Science*, 1997, **275**, 1102-1106.
15. R. S. Golightly, W. E. Doering and M. J. Natan, *ACS Nano*, 2009, **3**, 2859-2869.
16. M. D. Porter, R. J. Lipert, L. M. Siperko, G. Wang and R. Narayanan, *Chem. Soc. Rev.*, 2008, **37**, 1001-1011.

17. R. M. Jarvis and R. Goodacre, *Anal. Chem.* , 2003, **76**, 40-47.
18. Y. Wang, K. Lee and J. Irudayaraj, *J. Phys. Chem. C*, 2010, **114**, 16122-16128.
19. J. D. Driskell, K. M. Kwarta, R. J. Lipert, M. D. Porter, J. D. Neill and J. F. Ridpath, *Anal. Chem.*, 2005, **77**, 6147-6154.
20. K. Kneipp, H. Kneipp, I. Itzkan, R. R. Dasari and M. S. Feld, *J. Phys.: Condens. Matter*, 2002, **14**, R597.
21. W. R. Premasiri, D. T. Moir, M. S. Klempner, N. Krieger, G. Jones and L. D. Ziegler, *J. Phys. Chem. B*, 2004, **109**, 312-320.
22. W. R. P. I. S. Patel, D. T. Moir, and L. D. Ziegler, *J Raman Spectrosc*, 2008, **39**, 1660–1672.
23. S. Efrima and L. Zeiri, *Journal of Raman Spectroscopy*, 2009, **40**, 277-288.
24. J. A. D. Paul L. Stiles, Nilam C. Shah, and Richard P. Van Duyne, *Annu.Rev.Anal.Chem.*, 2008, **1**.
25. I. I. S. Anatoly V. Zayats, Alexei A. Maradudin, *Physics Reports*, 2005, **408** 131–314.
26. Yuling Wang, Sandeep Ravindranath and J. Irudayaraj, *Anal. Bioanal. Chem.*, 2011, **399**, 1271-1278.
27. R. J. L. Betsy Jean Yakes, John P. Bannantine, and Marc D. Porter1, *Clin Vaccine Immunol.*, 2008, **15**, 227-234.
28. E. C. Dreaden, A. M. Alkilany, X. Huang, C. J. Murphy and M. A. El-Sayed, *Chem. Soc. Rev*, 2012, **41**, 2740-2779.
29. P. U. Arumugam, H. Chen, S. Siddiqui, J. A. P. Weinrich, A. Jejelowo, J. Li and M. Meyyappan, *Biosens. Bioelectron.*, 2009, **24**, 2818-2824.
30. J. Voldman, *Annu. Rev. Biomed. Eng.*, 2006, **8**, 425-454.
31. P. U. Arumugam, H. Chen, A. M. Cassell and J. Li, *J. Phys. Chem. A*, 2007, **111**, 12772-12777.
32. L. U. Syed, J. Liu, A. K. Price, Y.-f. Li, C. T. Culbertson and J. Li, *Electrophoresis*, 2011, **32**, 2358-2365.
33. F. R. Madiyar, L. U. Syed, C. T. Culbertson and J. Li, *Electrophoresis*, 2013, **34**, 1123-1130.
34. F. R. Madiyar, L. U. Syed, P. Arumugam and J. Li, in *Advances in Applied Nanotechnology for Agriculture*, eds. B. Park and M. Appell, American Chemical Society, Washington DC, 2013, vol. 1143, ch. 6, pp. 109-124.
35. H. A. Pohl, *Dielectrophoresis: The Behavior of Neutral. Matter in Non-uniform Electric Fields*, Cambridge University Press,New York, , 1978.
36. G. H. Markx, Y. Huang, X.-F. Zhou and R. Pethig, *Microbiology*, 1994, **140**, 585-591.
37. A. E. M. Castellarnau, C. Madrid, A. Juárez,and J. Samitier, *Biophys J.* , 2006, **91**, 3937–3945.
38. M. P. Hughes, *Electrophoresis*, 2002, **23**, 2569-2582.
39. H.-C. C. I-Fang Cheng, Tzu-Ying Chen,Chenming Hu & Fu-Liang Yang, *Scientific Reports*, 2013.
40. U.-C. Schröder, A. Ramoji, U. Glaser, S. Sachse, C. Leiterer, A. Csaki, U. Hübner, W. Fritzsche, W. Pfister, M. Bauer, J. Popp and U. Neugebauer, *Anal. Chem.*, 2013, **85**, 10717-10724.
41. A. F. Chrimes, A. A. Kayani, K. Khoshmanesh, P. R. Stoddart, P. Mulvaney, A. Mitchell and K. Kalantar-zadeh, *Lab on a Chip*, 2011, **11**, 921-928.
42. S. Bhana, E. Chaffin, Y. Wang, S. R. Mishra and X. Huang, *Nanomedicine*, 2013, 1-14.
43. S. Bhana, B. K. Rai, S. R. Mishra, Y. Wang and X. Huang, *Nanoscale*, 2012, **4**, 4939-4942.
44. A. J. Bonham, G. Braun, I. Pavel, M. Moskovits and N. O. Reich, *J.Am.Chem.Soc.*, 2007, **129**, 14572-14573.

Integration of Nanostructured Dielectrophoretic Device and Surface-Enhanced Raman Probe for Highly Sensitive Rapid Bacteria Detection

Foram Ranjeet Madiyar[a], Saheel Bhana[b], Luxi Swisher[a], Xiaohua Huang[b], Christopher Culbertson[a], and Jun Li[a]

Figure 1

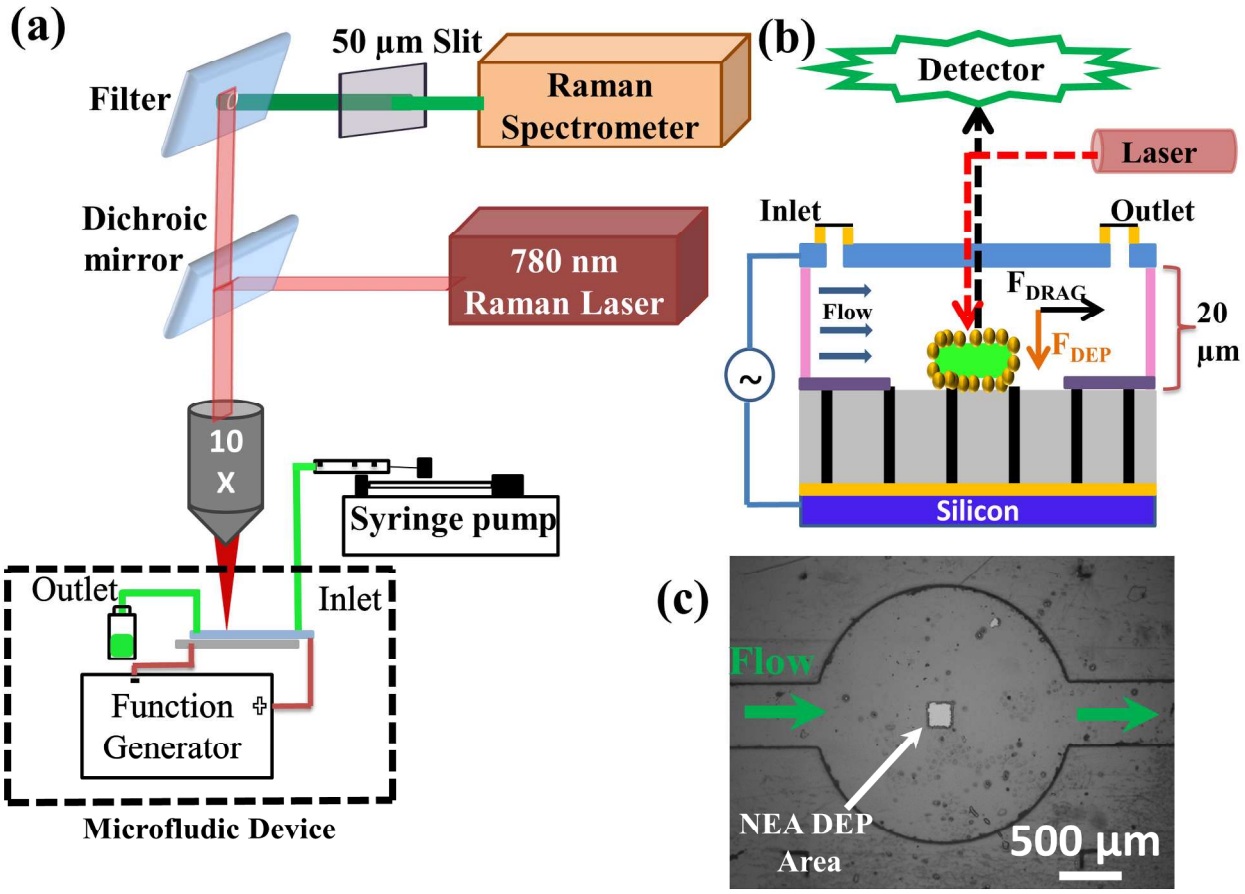

Figure 1. Schematic of the microfluidic dielectrophoresis device under a Raman microscope for bacteria detection. (a) The overall experimental setup of a confocal Raman microscope equipped with a 780 nm laser and a 10X objective lens. (b) Enlarged schematic view of DEP capture of the bacteria bind with oval-shaped SERS nanotags for the Raman detection with a portable Raman probe. (c) Optical microscope image taken under 4X magnification showing the microfluidic channel and the active square at the center.

Figure 2

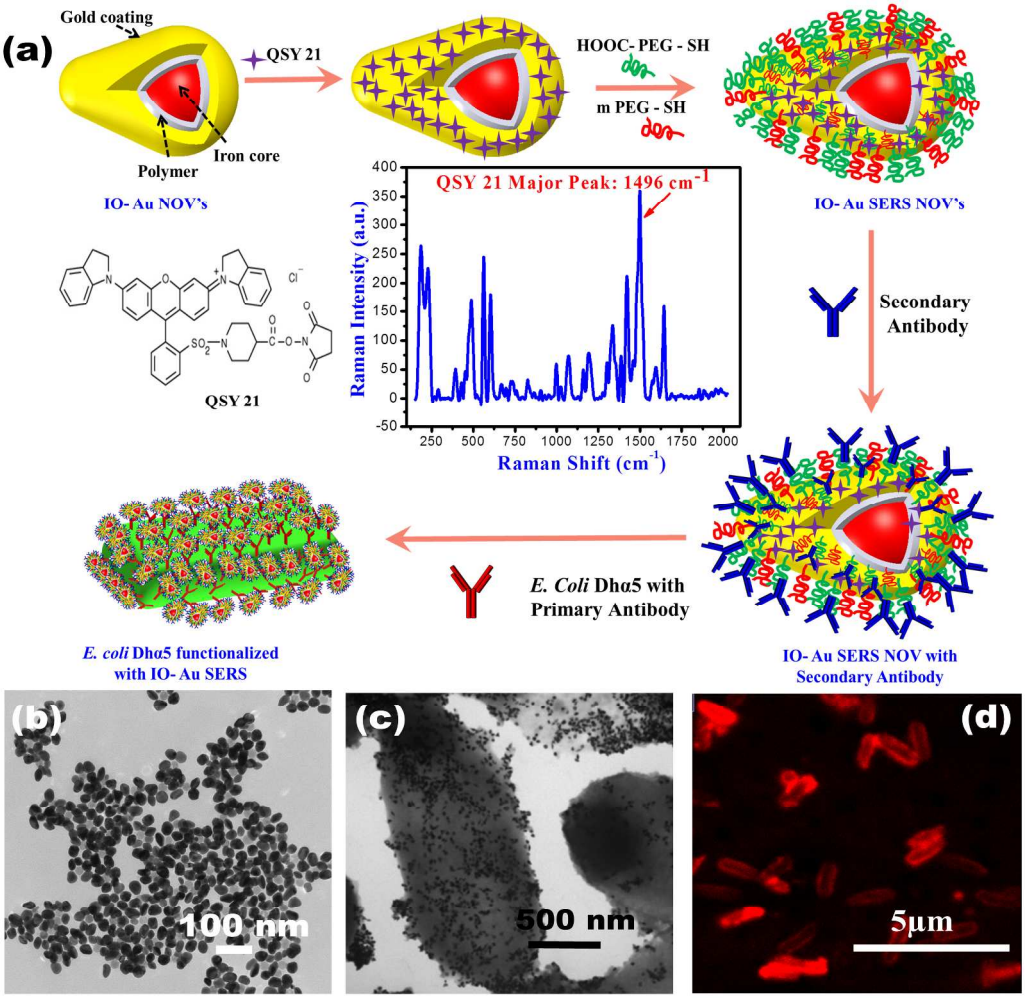

Figure 2. (a) Schematic procedures for preparation of QSY 21 derivatized iron oxide-gold core-shell nano-ovals (IO-Au NOVs) as nanotags for SERS measurements and their attachment to *E. coli* bacterial cells through a FITC-labeled primary antibody and a Alexa 555 labeled secondary antibody. TEM images of (b) the starting IO-Au NOVs and (c) E. coli DHα5 bacterial cells attached with antibody-functionalized IO-Au NOVs. (d) Confocal fluorescence image of Alexa 555 in *E. coli* DHα5 bacterial cells attached with antibody-functionalized IO-Au NOVs. Alexa 555 was attached to the secondary antibody.

Figure 3

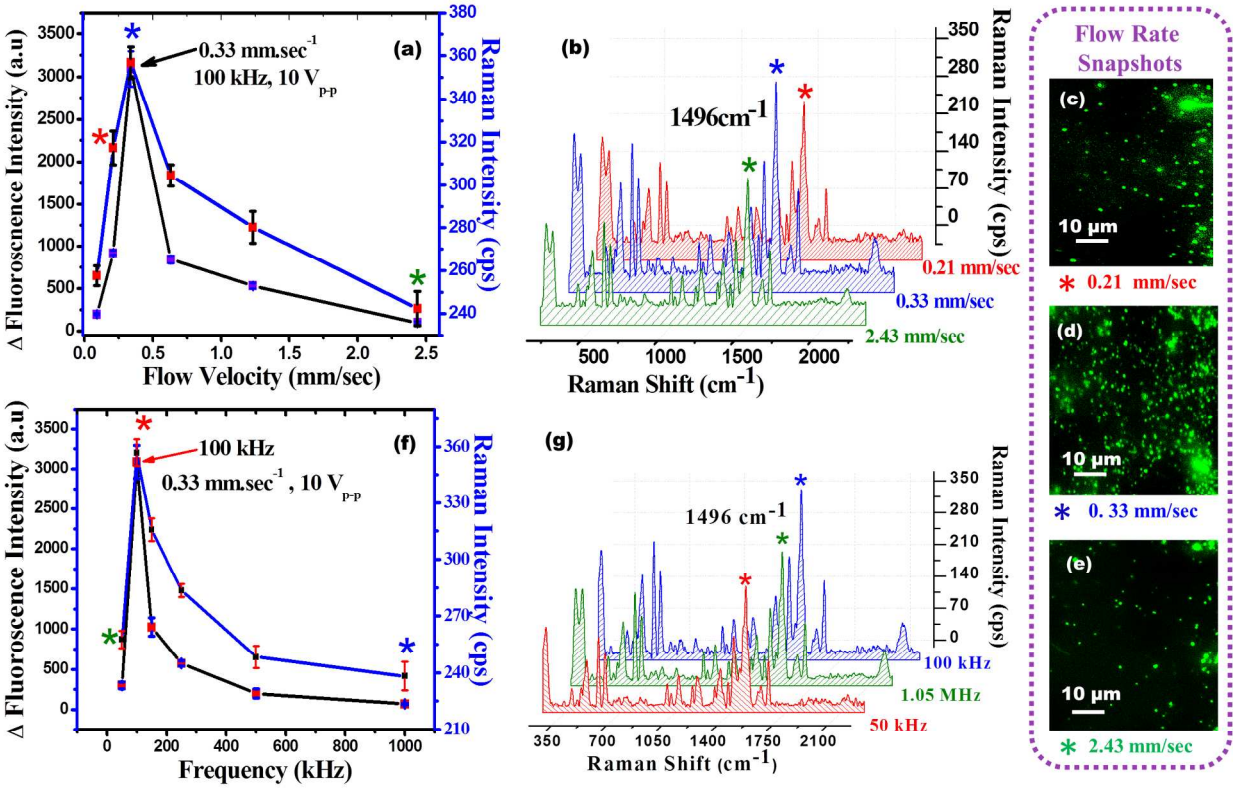

Figure 3. Assessing DEP capture of 5.3 x 10^5 cfu/mL *E. coli* cells with fluorescence and Raman measurements at various flow velocity and AC frequency. (a) The study of flow velocity at fixed frequency (100 kHz) and voltage (10 V_{pp}). (b) Representative Raman spectra of QSY-21 and (c-e) corresponding snapshots from the fluorescence videos after 50 s of DEP capture of IO-Au NOV labeled *E. coli* cells at flow velocity of 0.21 mm/sec (red star), 0.33 mm/sec (blue star), and 2.43 mm/sec (green star). (f) The study of AC frequency at fixed flow velocity (0.33 mm/s) and voltage (10 V_{pp}). (g) Representative Raman spectra of QSY-21 after 50 s of DEP capture of IO-Au NOV labeled *E. coli* cells at 50 kHz (green star), 100 kHz (red star), and 1,000 kHz (blue star).

Figure 4

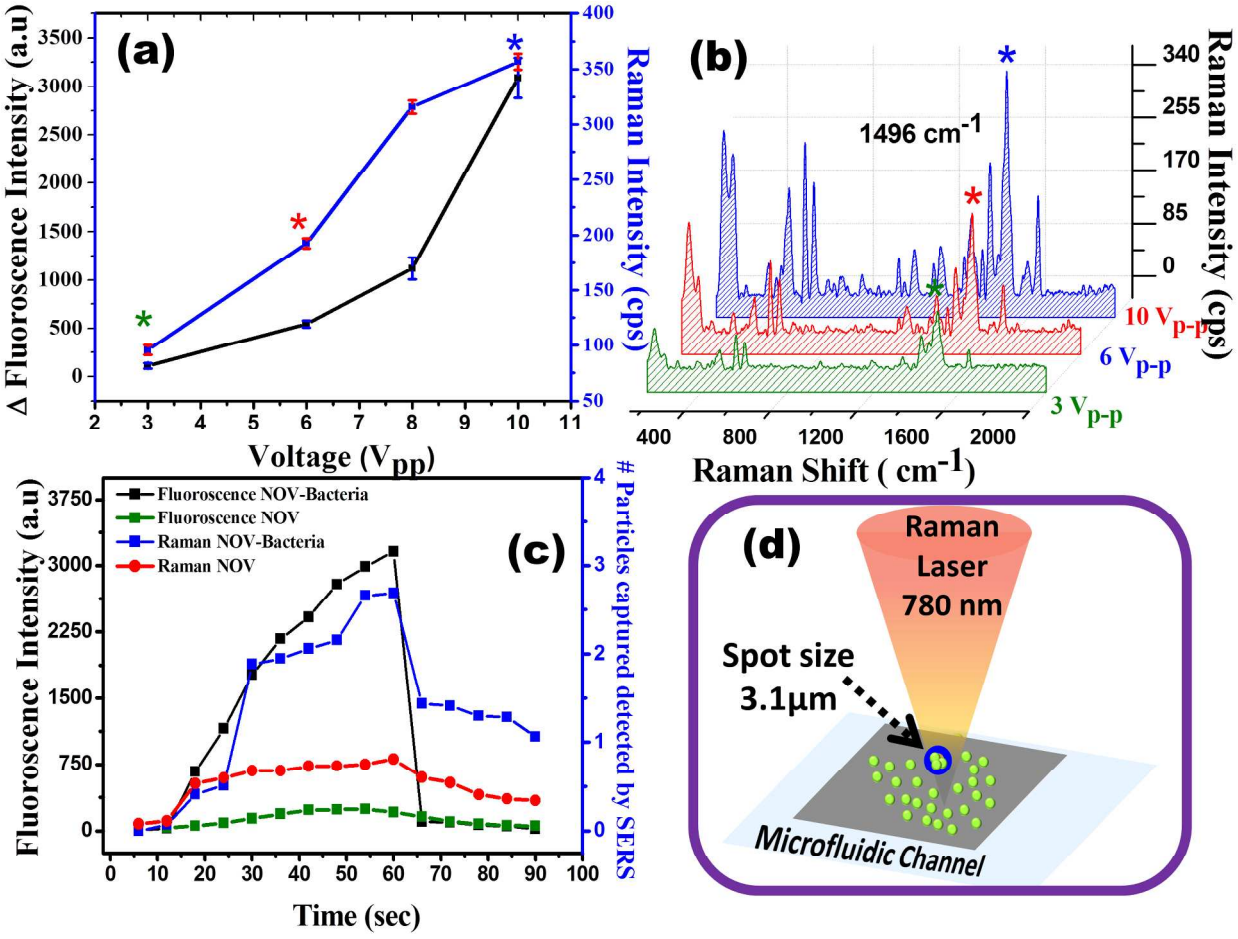

Figure 4. Assessing DEP capture of 5.3 x 10^5 cfu/mL *E. coli* cells with fluorescence and Raman measurements with varying voltage and time. (a) The study of voltage at fixed flow velocity (0.33 mm/s) and AC frequency (100 kHz). (b) Representative Raman spectra of QSY-21 after 50 s of DEP capture of IO-Au NOV labeled *E. coli* cells at 3 V_{pp} (green star), 6 V_{pp} (red star), and 10 V_{pp} (blue star). (c) The kinetic curve during DEP capture of 4 x10^3 cfu/ml IO-Au NOV labeled *E. coli* cells, with the AC voltage off in the first ~15 s, on from 15 to 65 s, and then off beyond 65 s. During the 50 s period with the voltage on, bacteria accumulate on the electrode surface by DEP capture and give increasing fluorescence and Raman intensities, which are immediately released into the fluid flow when the AC voltage is turned off at 65 s. (d) Schematic diagram to illustrate the 3.1 μm laser focal spot size relative to the bacterial size.

Figure 5

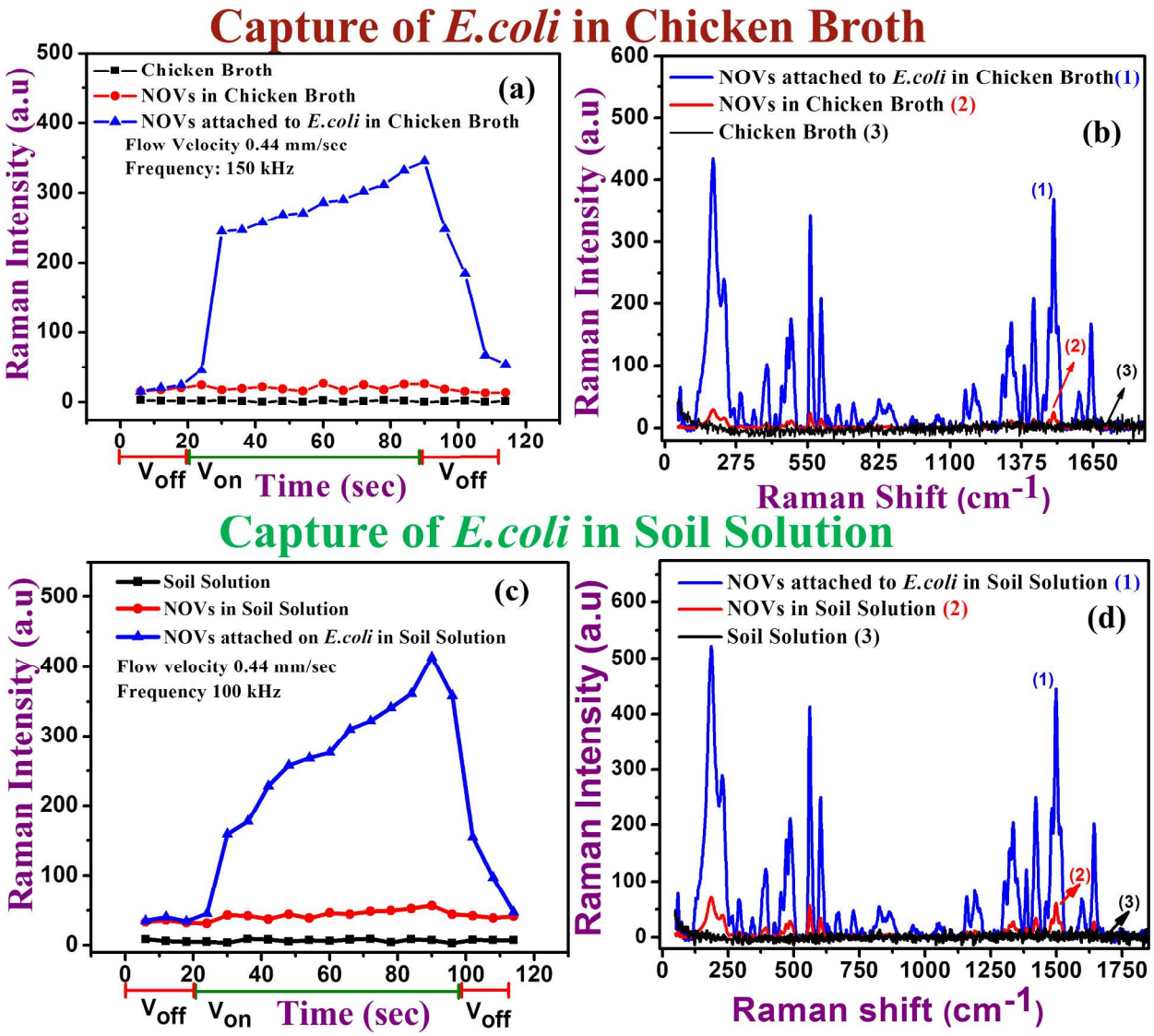

Figure 5. Assessing DEP capture of *E. coli* cells with fluorescence and Raman measurements in different complex matrices. (a) The kinetic curve of DEP capture of *E. coli* cells in a chicken broth at 10 V_{pp}, 0.44 mm/s flow velocity, and 150 kHz AC frequency. (b) Representative Raman spectra of QSY-21 in chicken broth after 50 s of DEP capture of IO-Au NOV labeled *E. coli* cells. (c) The kinetic curve of DEP capture of *E. coli* cells in a soil solution at 10 V_{pp}, 0.44 mm/s flow velocity, and 150 kHz AC frequency. (d) Representative Raman spectra of QSY-21 in soil solution after 50 s of DEP capture of IO-Au NOV labeled *E. coli* cells. The measurements from blank matrix, NOV spiked matrix (1.4 x 10^{10} NOVs/ml), and NOV-bacteria spiked matrix (5 x 10^{5} cfu/ml) are presented in each panel.

Figure 6:

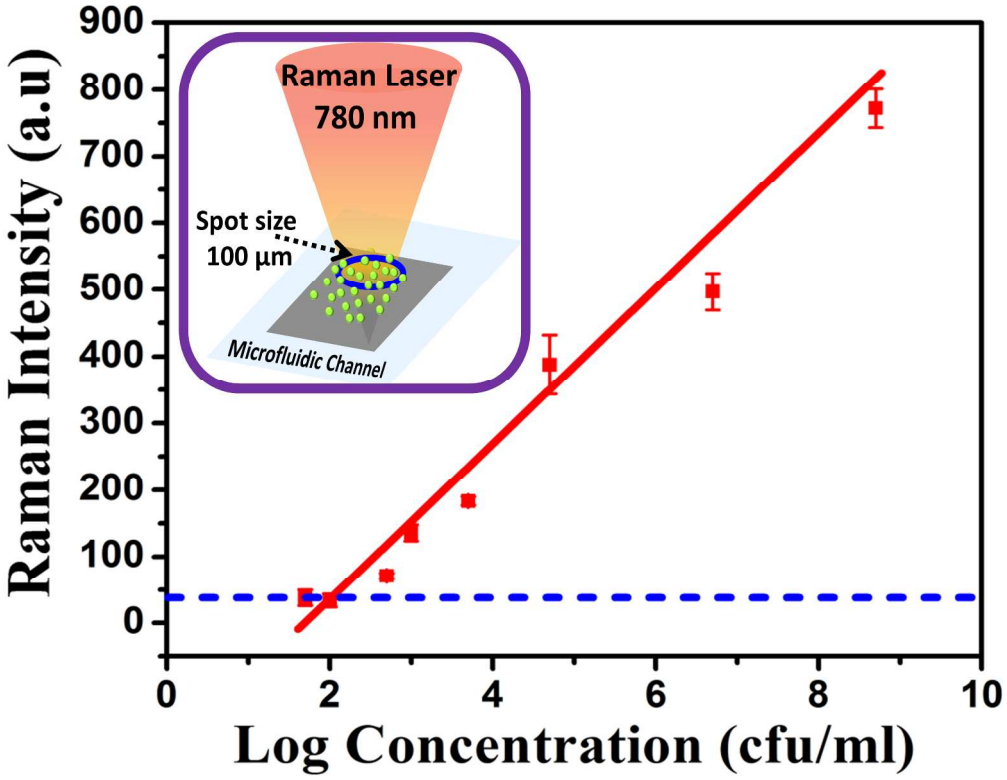

Figure 6. The Raman intensity after 50 s of DEP capture from the bacteria solution with the concentration varying from 5 cfu/mL to 1.0 x 10^9 cfu/mL. The Raman measurements were carried out by focusing the laser beam within the 200 µm x 200 µm active DEP area with a ProRaman L portable Raman system (Enwave Optronics).Inset shows that 100 µm diameter laser focal spot aligned with 200 µm x 200 µm active DEP area